

Single-Event Effects Induced by Monoenergetic Fast Neutrons in Silicon Power UMOSFETs

Saulo G. Alberton¹, Alexis C. Vilas-Bôas¹, Marcilei A. Guazzelli¹, *Member, IEEE*, Vitor A. P. Aguiar¹, Matheus S. Pereira¹, Nemitala Added¹, Claudio A. Federico¹, Tássio C. Cavalcante, Evaldo C. F. Pereira Júnior, Rafael G. Vaz, Odair L. Gonzalez¹, Jeffery Wyss², Alessandro Paccagnella², *Senior Member, IEEE*, Nilberto H. Medina¹, *Member, IEEE*

Abstract—The trench gate or U-groove MOSFET (UMOSFET) has become widely adopted as a semiconductor device globally, gradually replacing the traditional vertical double-diffused MOSFET (DMOSFET) in many applications. Evaluating the reliability of UMOSFETs regarding neutron-induced radiation effects is crucial for understanding their response to ubiquitous atmospheric neutrons. This study presents comparative experimental and computational results of Single-Event Effects induced by monoenergetic fast neutrons in UMOS and DMOS power transistors. Experiments demonstrate that UMOSFETs exhibit premature particle-induced avalanche multiplication effects compared to similarly rated DMOSFETs, which may favor destructive radiation effects, such as Single-Event Burnout, when operating in the terrestrial radiation environment.

Index Terms—Power transistor, UMOSFET, trench MOSFET, DMOSFET, radiation effects, Single-Event Effect, neutrons, nuclear reaction, charge collection

I. INTRODUCTION

VERTICAL DOUBLE-DIFFUSED MOSFETs (DMOSFETs) are traditionally used in power electronics and are widely known to suffer both non-destructive and destructive Single-Event Effects (SEEs) induced by radiation. Non-destructive SEE mainly includes Single-Event Transient (SET) [1]. Destructive SEEs in DMOSFETs include Single-Event Burnout (SEB) and Single-Event Gate Rupture (SEGR) modes, in which both can be induced by heavy ions [2]–[4] in outer space, and by neutrons [5] in terrestrial environments. Currently, the trench gate or U-groove MOSFETs

This study was financed in part by the Coordenação de Aperfeiçoamento de Pessoal de Nível Superior - Brasil (CAPES) - Financial Code 001; CNPq (Nos. 404054/2023-4 and 422360/2023-6); FAPESP (No. 2023/16053-8); FINEP (No. 01.12.0224.00); and INCT-FNA (No. 464898/2014-5).

S. G. Alberton is with the Instituto de Física, Universidade de São Paulo, São Paulo, SP, Brazil, and also with the Dipartimento di Ingegneria dell'Informazione, Università degli Studi di Padova, Padova 35131, Italy (e-mails: alberton@if.usp.br, albertonsg@dei.unipd.it).

A. C. Vilas-Bôas and M. A. Guazzelli are with the Centro Universitário FEI, São Bernardo do Campo, SP, Brazil.

V. A. P. Aguiar, M. S. Pereira, N. Added, and N. H. Medina are with the Instituto de Física, Universidade de São Paulo, São Paulo, SP, Brazil.

C. A. Federico, T. C. Cavalcante, E. C. F. Pereira Júnior, R. G. Vaz, and O. L. Gonzalez are with the Instituto de Estudos Avançados, São José dos Campos, SP, Brazil.

J. Wyss is with the Dipartimento di Ingegneria Civile e Meccanica, Università degli Studi di Cassino e del Lazio Meridionale, Cassino 03043, Italy, and also with the Istituto Nazionale di Fisica Nucleare, Padova 35131, Italy.

A. Paccagnella is with the Dipartimento di Ingegneria dell'Informazione, Università degli Studi di Padova, Padova 35131, Italy.

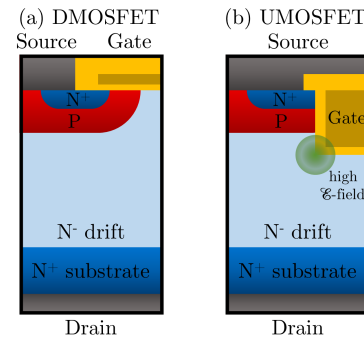


Fig. 1. Half-cell cross sections of representative (a) vertical double-diffused MOSFET (DMOSFET) and (b) U-groove MOSFET (UMOSFET).

(UMOSFET) have been supplanting the DMOSFET technology in numerous applications, establishing their position as one of the most widely used semiconductor devices worldwide [6]. UMOSFETs have demonstrated superior electrical performance due to low ON-resistance and gate charge, high-frequency switching capabilities, high epitaxial current uniformity, and can be fabricated with much higher transistor cell densities in comparison to DMOSFETs [6]–[9]. Figure 1 depicts a illustration of both DMOS and UMOS structures.

Although extensive radiation effects studies have been conducted in the traditional DMOSFET technology over the past decades, there are relatively few studies published on power FETs with alternative architectures [10]. It is claimed that there is currently a lack of detailed and comparative experimental studies on the radiation response and charge collection mechanisms of similarly rated UMOS and DMOS power FETs [11]. Radiation hardness studies on silicon (Si) UMOSFETs are relatively scarce and have primarily focused on front-side irradiation with high-energy heavy ions for space applications [12]–[18]. This physical scenario is substantially different from neutron irradiation, which can produce multiple secondary ionizing particles with complex angular and energy distributions through stochastic nuclear reactions with the atomic nuclei of material constituents of the device. Evaluating the reliability of prominent UMOSFETs under radiation effects induced by ubiquitous neutrons in Earth's atmospheric environment is relevant for automotive applications (electric and autonomous cars, traction) and crucial for avionics applications, where neutron fluence rates can be hundreds of times more intense than at ground level. Preliminary studies indicate that a UMOSFET device may exhibit enhanced avalanche mul-

tiplication effects compared to a similarly rated DMOSFET when exposed to alpha particle and neutron irradiation [19], [20], suggesting potential unique risks. Very recent research has experimentally investigated destructive effects induced by neutrons provided by spallation facilities in Si-based UMOS-FETs, finding superior SEB vulnerability [21]. The present study represents an additional step toward assessing the long-term reliability of UMOSFETs operating in terrestrial radiation environments by systematically investigating their charge collection response to monoenergetic fast neutron irradiation.

This study presents comprehensive experimental and computational investigations of the SEE response and charge collection mechanisms on similarly rated Si UMOS and DMOS power FETs exposed to monoenergetic fast neutrons provided by a Deuterium-Tritium (D-T) neutron generator. Although D-T neutrons are not fully representative of atmospheric neutrons, they provide valuable insights into the physical aspects of complex nuclear reaction processes and corresponding charge collection mechanisms in power devices. The fast neutron energy was precisely measured by using a Silicon Surface Barrier (SSB) particle detector, and the collected charge spectra of the devices under test (DUTs) irradiated by D-T neutrons were measured and comparatively analyzed. The radiation transport toolkit G4SEE [22] was utilized to provide a detailed description of the nuclear reaction channels involved, validating its use for modeling neutron-induced SEE response in Si power FETs of distinct technologies, and supporting data analysis. Finally, based on experimental results and numerical calculations, one describes the mechanism that may favor avalanche multiplication effects induced by neutrons in Si UMOSFET and potentially promote the occurrence of SEB destructive failure mode in terrestrial radiation environments.

II. EXPERIMENTAL METHODS

A. Particle Source

Monoenergetic fast neutrons were produced by the D-T Thermo ScientificTM MP 320 Neutron Generator located at the *Instituto de Estudos Avançados* (IEAv), São José dos Campos, Brazil. This D-T neutron generator is capable to provide a monoenergetic neutron beam with approximately 14 MeV and a typical neutron yield of about 10^8 neutrons/s.

B. Tested Devices

Similarly rated Si-based UMOS and DMOS power FETs, as well as of a SSB particle detector, were irradiated under monoenergetic fast neutrons provided by the IEAv D-T Neutron Generator in a total of two experimental campaigns. The SSB detector, with an active area and thickness of 100 mm^2 and $100 \mu\text{m}$, respectively, was especially used for measuring the neutron beam energy, as described in Section II-C. In the first experimental campaign, one UMOSFET and one DMOSFET with rated breakdown voltages (BV_{rated}) of 60 V and 55 V, respectively, were irradiated (see Table I). In the second campaign, several similarly rated UMOS and DMOS power FETs, with BV_{rated} ranging from 40 V up to 150 V, were investigated (see Table II). The actual breakdown voltages

(BV_{DS}) of the DUTs are also provided in the corresponding tables.

TABLE I
UMOS AND DMOS POWER FETs IRRADIATED WITH FAST NEUTRONS IN THE FIRST EXPERIMENTAL CAMPAIGN

Device	Technology	BV_{rated} [V]	BV_{DS} [V]	Die area [mm^2]
IXFA220N06T3	UMOS	60	69.44(5)	27.5(4)
IRLZ34NPBF	DMOS	55	69.84(29)	1.52(9)

BV_{rated} is the nominal breakdown voltage, rated according manufacturer, and BV_{DS} is the mean value (and standard deviation) of the actual breakdown voltage measured across devices from the same batch.

TABLE II
UMOS AND DMOS POWER FETs IRRADIATED WITH FAST NEUTRONS IN THE SECOND EXPERIMENTAL CAMPAIGN

Device	Technology	BV_{rated} [V]	BV_{DS} [V]	Die area [mm^2]
TPH6R004PL	UMOS	40	45.95(7)	5.5(5)
TPH7R506NH	UMOS	60	73.3(12)	6.55(24)
TPH4R10ANL	UMOS	100	114.5(7)	8.2(6)
TPH3300CNH	UMOS	150	164.0(10)	6.79(25)
IRF1104PBF	DMOS	40	46.75(7)	21.2(9)
IRFZ44ESPBF	DMOS	60	67.65(7)	14.58(28)
IRFR120NPBF	DMOS	100	115.7(6)	6.92(13)
IRFR24N15DPBF	DMOS	150	159.5(6)	11.3(5)

BV_{rated} is the nominal breakdown voltage, rated according manufacturer, and BV_{DS} is the mean value (and standard deviation) of the actual breakdown voltage measured across devices from the same batch.

C. Test Methodology

Charge collection spectroscopy [23], [24] of the DUTs was performed by using Nuclear Instrumentation Module (NIM) electronics, which primarily consisted of power supply (ORTEC 710 Quad 1-kV Bias Supply), charge-sensitive preamplifier (ORTEC A142B, CAEN A1422) and a high-resolution digitizer (CAEN N6725). The charge-sensitive preamplifier converts the current signal from the DUT into a voltage signal with a fast rise time ($\sim\text{ns}$) and a slow fall time ($100 \mu\text{s}$), where the amplitude is proportional to the collected charge. The digitizer operates with a sampling rate of 250 MSa/s per channel, enabling precise measurement of the preamplifier's signal amplitude and, therefore, the collected charge. The electronic acquisition system was calibrated by using a precision charge pulse generator and 5.486 MeV alpha particles emitted by a ^{241}Am radiation source. The charge collected due to the nuclear reaction fragments produced by the interaction of fast neutrons with the DUT materials were continuously measured during frontal irradiation at a standard axial position. During measurements, trigger levels were set as low as possible to minimize system dead time.

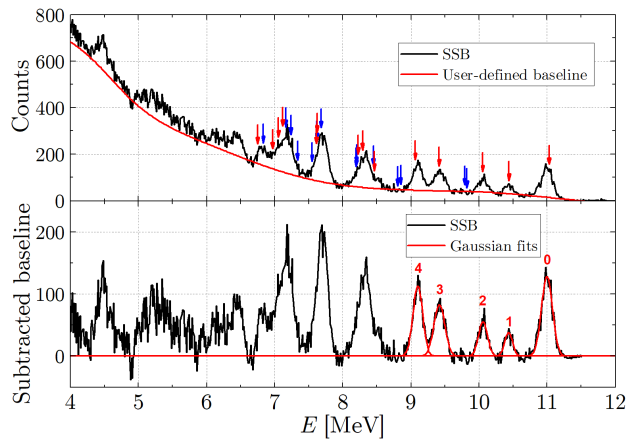


Fig. 2. Energy spectrum measured from the interaction of D-T neutrons with a fully depleted SSB detector at the predefined irradiation position. The spectrum is presented both before (top) and after user-defined baseline subtraction (bottom). Arrows indicate predicted energy levels for ^{25}Mg (red) and ^{28}Al (blue) nuclei, based on the measured neutron energy value.

1) *Neutron Energy Measurement*: The fully depleted SSB detector was used to measure the neutron energy at the standard axial irradiation position. Since high energy protons produced in $n + \text{Si} \rightarrow p + \text{Al}$ reactions (usually represented as $\text{Si}(n,p)\text{Al}$ in compact notation) are very likely to escape from the SSB detector volume, the relative contribution of this reaction channel to the measured charge spectrum is greatly suppressed compared to the (n,α) reaction channel [25]. This fact was used to measure the neutron beam energy at the predefined standard irradiation position through the $^{28}\text{Si}(n,\alpha)^{25}\text{Mg}$ nuclear reaction. From energy conservation in the laboratory reference frame, the neutron energy can be written as:

$$E_n = E_{\text{peak}} + E_{\text{exc}} - Q, \quad (1)$$

in which $E_{\text{peak}} = E_{\alpha} + E_{^{25}\text{Mg}}$ is the sum of energies of the respective ejectile (α -particle) and recoil (^{25}Mg) outgoing particles detected by the SSB detector, E_{exc} is the excitation energy of the ^{25}Mg nucleus, and the Q -value is the mass change in units of energy. Since the Q -value for the $^{28}\text{Si}(n,\alpha)^{25}\text{Mg}$ reaction [26] and the E_{exc} values of the ^{25}Mg nucleus [27], [28] are known with a high precision, the accuracy and precision of the mean neutron energy measurement are primarily determined by E_{peak} . In Fig. 2, the energy spectrum resulting from the interaction of the fast neutrons with the fully depleted SSB detector is shown. A user-defined baseline subtraction was applied to the original SSB energy spectrum, and Gaussian curve fits were performed on the higher energy peaks assigned to several ^{25}Mg energy levels. In order to avoid complications introduced by overlapping peaks assigned to different nuclei, a weighted mean neutron energy of $E_n = 13.68(3)$ MeV was obtained by selecting the peaks assigned to the ground state and the first four excited states of ^{25}Mg . As a reference, Fig. 2 also shows the energy level predictions for the ^{25}Mg and ^{28}Al nuclei based on the estimated E_n value, demonstrating a high level of accuracy.

2) *Neutron-induced SEE Experiments*: The DUTs were stacked for front-side irradiation at the predefined stan-

dard axial position with beam fluences typically reaching 10^{10} neutrons/cm 2 . During experimental campaigns, the DUTs were set in the OFF mode, *i.e.*, with the gate-source voltage $V_{\text{GS}} = 0$ V and drain-source voltage $V_{\text{DS}} > 0$ V.

In the first experimental campaign, the DUTs (see Table I) were set at $V_{\text{DS}} = 50$ V, below their rated breakdown voltages (at $V_{\text{DS}}/BV_{\text{DS}} \approx 71.80(21)\%$, in average), to prevent avalanche multiplication. In order to achieve the typical fluence level, each DUT was irradiated with neutrons for at least 20 hours and the SEE signals were treated by using an ORTEC 142B charge-sensitive preamplifier in single-channel mode, resulting in a low level of electronic noise.

On the other hand, in the second experimental campaign, the DUTs (see Table II) were set at $V_{\text{DS}} = BV_{\text{rated}}$, their maximum rated drain-source voltage (at $V_{\text{DS}}/BV_{\text{DS}} \approx 87.8(27)\%$, in average), to systematically compare the potential avalanche multiplication effects between the UMOS and DMOS technologies. During this campaign, the DUTs were simultaneously irradiated and the SEE signals were treated in octal-channel mode by using a CAEN A1422 charge-sensitive preamplifier.

III. RESULTS

No destructive SEEs were observed during the experimental campaigns. Since only SEEs of the SET type were detected, we refer to them simply as SEEs. The observation of exclusively non-destructive SEEs is attributed to the limited linear energy transfers (LETs) of the reaction products generated from D-T neutron interactions in Si, which are insufficient to induce destructive effects under the test conditions. For instance, the reaction channel $^{28}\text{Si}(n,\alpha)^{25}\text{Mg}$ can produce alpha particles with energies up to approximately 10.9 MeV and ^{25}Mg nuclei with energies up to about 3.5 MeV. By using the SRIM code [29], the corresponding surface LET values of these particles in Si material are estimated to be $0.37 \text{ MeV}\cdot\text{cm}^2\cdot\text{mg}^{-1}$ and $8.6 \text{ MeV}\cdot\text{cm}^2\cdot\text{mg}^{-1}$, respectively.

The vulnerability of the DUTs to neutron-induced radiation effects was evaluated in terms of SEE cross section, σ , defined as the ratio of the total number of detected SEEs to the particle beam fluence of each test run. The SEE cross section is related to the probability of a SEE occurrence and indicates the fraction of the device's sensitive area that effectively contributes to triggering SEEs. In order to directly compare the charge spectra of the DUTs induced by D-T neutrons, we preferably evaluated the differential cross section distributions ($d\sigma/dE$), which is the differential counts normalized per beam fluence and energy bin width (dE), normalized by their die areas. Normalizing the SEE cross sections by die area enable us to assess the technology's SEE vulnerability independently of device's die area dimensions and is equivalent to represent their σ as if all DUTs have an equivalent die area of 1 cm^2 . Additionally, for a more rigorous comparative analysis, it is useful to define the cross section from a given energy threshold E_{th} :

$$\sigma[E_{\text{th}}] = \int_{E_{\text{th}}}^{\infty} \frac{d\sigma}{dE} dE. \quad (2)$$

A. First experimental campaign: a case study

Figure 3 shows results for the similarly rated UMOS and DMOS power FETs irradiated below their respective BV_{rated} values. In Fig. 3, the differential cross section distributions show that the UMOSFET device is more susceptible to SEEs compared to the DMOSFET device. This susceptibility can be explicitly quantified by integrating the $d\sigma/dE$ distributions. By setting a common energy threshold of $E_{th} = 1$ MeV in (2), the SEE cross sections for the UMOSFET and DMOSFET devices are found to be $4.5(2) \times 10^{-6} \text{ cm}^2$ and $2.3(2) \times 10^{-7} \text{ cm}^2$, respectively. Nevertheless, the SEE cross sections are not inherently a feature of the device's technology but rather a general characteristic of the electronic component itself. Although the UMOS device is more susceptible to SEE than the DMOS device, calculating the SEE cross section normalized per die area can provide a better understanding of the SEE susceptibility across technologies. For the same energy threshold of $E_{th} = 1$ MeV, the normalized cross section values for the UMOS and DMOS technologies are $1.63(7) \times 10^{-5} \text{ cm}^2$ and $1.53(14) \times 10^{-5} \text{ cm}^2$, respectively. These findings suggest that similarly rated low-voltage UMOS and DMOS power FETs with equivalent die areas exhibit comparable susceptibilities to SEEs induced by D-T neutrons when biased significantly below their BV_{rated} values. As shown in Fig. 3, the match between the normalized distributions indicates that DUTs have nearly equivalent sensitive widths, despite significant architectural differences. This observation motivated the proposal of a simplified computational model for neutron-induced SEE in Si power FETs, presented in Section III-B.

Beyond the susceptibility to non-destructive SEEs, another important point to note is that, despite applying a drain-source voltage ($V_{DS} = 50$ V) below the BV_{rated} of the DUTs, the UMOSFET exhibited a few events of relatively high charge collection. For example, the UMOSFET detected SEEs of approximately 0.63 pC, corresponding to 14.2 MeV. Since this value exceeds even the maximum collected charge in the fully depleted SSB detector, this observation suggests that the UMOSFET may experience avalanche multiplication induced by fast neutron irradiation, according to previous observations under alpha particle irradiation at similar V_{DS} levels [19]. A second experimental campaign was conducted in order to further investigate and clarify this possibility.

B. Second experimental campaign: systematic study

In the second experimental campaign, several similarly rated UMOS and DMOS power FETs, with BV_{rated} ranging from 40 V up to 150 V, were investigated (see Table II). In Fig. 4, the experimental normalized differential cross section distributions for DMOS (blue lines) and UMOS (red lines) are shown. A remarkable result is the fact that neutron-induced SEEs corresponding to collected charge values higher than 1 pC were detected for both 100 V and 150 V UMOSFETs. Comparatively, very few events with such high magnitude of collected charge were observed for the 150 V DMOSFET, whereas no such events were observed for the 100 V DMOSFET. The maximum experimental charge collected by

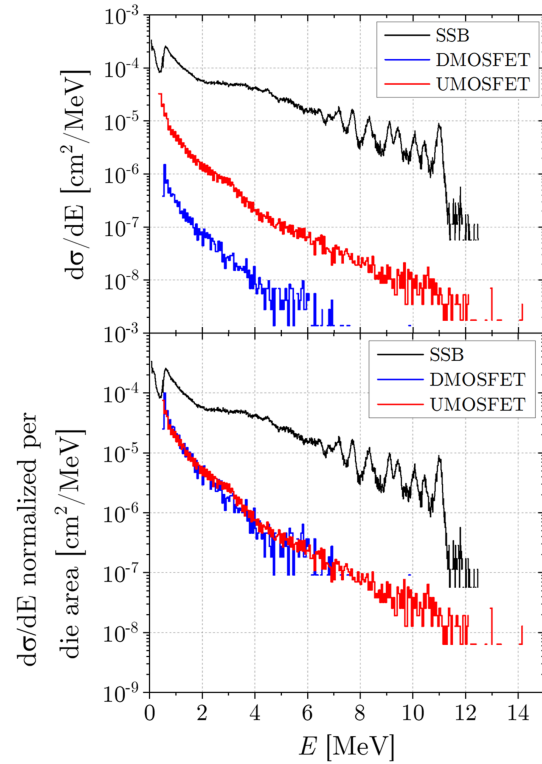


Fig. 3. Differential SEE cross section (top) and differential SEE cross section normalized per die area (bottom) distributions for a UMOSFET ($BV_{rated} = 60$ V) and a DMOSFET ($BV_{rated} = 55$ V) irradiated at $V_{DS} = 50$ V in the first experimental campaign.

100 V and 150 V UMOSFETs is substantially higher than the maximum charge collected by the SSB detector, revealing that avalanche multiplication phenomena occurred in these DUTs. Alternatively, when expressed in terms of deposited energy in Si, SEEs associated with these high-charge events correspond to energy values that exceed the maximum kinetic energy initially available from impinging D-T neutrons by a factor of approximately two. Compared to similarly-rated DMOSFETs, these facts show that UMOSFETs experience enhanced avalanche multiplication and are more prone to this phenomenon, which is observed prematurely in devices with comparatively lower voltage ratings.

Computational simulations were performed by using the G4SEE toolkit [22] to clarify the interpretation of the energy spectra measured in the second experimental campaign. The MOSFETs were modeled according to a generic FET structure based on microscopic analysis of several DUT samples. The modeled structure consists of a 5 μm -thick aluminium (Al) metallization layer and a Si rectangular parallelepiped (RPP) sensitive region on the top of a 100 μm -thick Si bulk. The sensitive region is composed by a typical 2 μm -thick p-base layer [30] and a depletion layer. The depletion region width is estimated according to [9]:

$$W_d = \left[\frac{2 \epsilon_{Si} V_{DS}}{q N_d} \right]^{1/2}, \quad (3)$$

in which ϵ_{Si} is the Si permittivity, V_{DS} is the drain-source applied voltage, q is the electron charge, and N_d is the doping

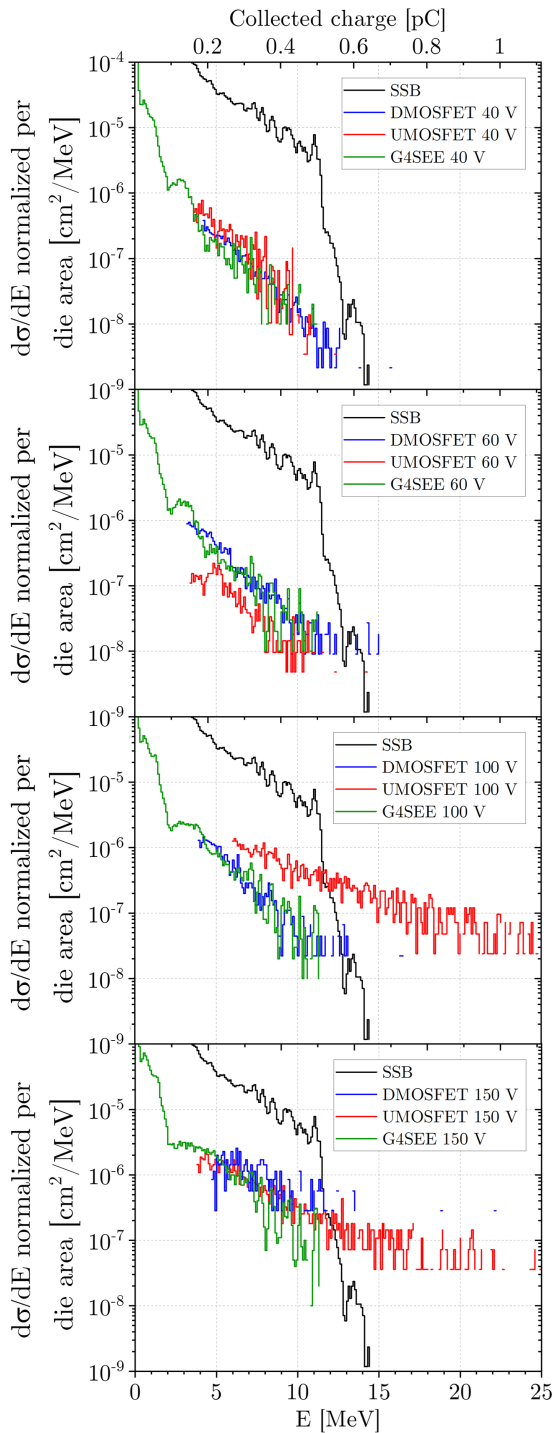


Fig. 4. Differential SEE cross section distributions normalized by die area for similarly rated DMOSFETs and UMOSFETs ranging from 40 V to 150 V, irradiated at nominal voltage ($V_{DS} = BV_{rated}$). All graphs share the same abscissa axis. Computational results obtained with G4SEE toolkit [22] are also included (see text for discussion).

concentration in the epitaxial region, which is estimated from the Baliga's semi-empirical approximation [9]:

$$N_d = \left[\frac{4.45 \times 10^{13}}{BV_{DS}} \right]^{4/3}. \quad (4)$$

For simplicity, it is also assumed that the ratio between the

actual and rated drain-source breakdown voltage is defined through the Edge Termination Relation [9]:

$$BV_{DS} = \frac{BV_{rated}}{0.8}. \quad (5)$$

Therefore, by using the BV_{rated} values, one can estimate the depletion region width of the DUTs by inserting (5) and (4) in (3). The uncertainty of (5) in estimating sensitive widths from measured breakdown voltages is approximately 5%, which is negligible compared to the dominant uncertainties in the neutron cross section evaluations from Geant4 libraries [31], on which G4SEE is based. Consequently, the computational results serve as reference for comparison with experimental data. In our simulations, the standard G4EmStandardPhysics_option4 module was adopted for the electromagnetic physics, and the G4HadronElasticPhysicsHP (high precision elastic) and G4HadronPhysicsFTFP_BERT_HP (high precision inelastic) modules were adopted for the hadronic physics. Additionally, the production range cuts for secondary particles were set 1 mm for gamma-rays, 1 μ m for electrons and positrons, and 100 nm for all other particles.

Figure 4 includes the comparison between experimental data and computational results obtained with G4SEE (green lines). Except for the SEE responses of 100 V and 150 V UMOSFETs, a relatively good agreement between the experimental and computational simulations is generally obtained. The Geant4 libraries [31] can simulate nuclear reaction channel probabilities, the angular distribution of secondary particle emissions, and their ionizing energy loss through matter. However, they do not account for semiconductor device operation or detailed carrier transport physics, such as avalanche multiplication. Therefore, assuming that the computational modeling adopted is decent, the agreement between computational and experimental results support the claim that few or no avalanche multiplication effects are occurring on a specific DUT. For instance, the overall good agreement between computational and experimental results for the DMOSFETs confirm that D-T neutrons do not induce significant avalanche multiplication effects in this technology under the test conditions of the present study. On the other hand, the notable discrepancies observed for the 100 V and 150 V UMOSFETs confirm the occurrence of avalanche multiplication in this technology.

A detailed analysis of the computational results can be conducted to assess the secondary particles that are primarily responsible for causing SEEs induced by D-T neutrons in the DUTs. Figure 5 illustrates a direct comparison between experimental data and computational prediction for the 100 V DMOSFET presented as a stacked histogram, with the relative energy deposition contribution for each reaction channel classified event by event. The four most probable nuclear reaction channels resulting from the interaction of D-T neutrons with silicon are shown, suggesting that the $^{28}\text{Si}(n,\alpha)^{25}\text{Mg}$ nuclear reaction is the dominant failure mode for deposited energies higher than approximately 2 MeV. Furthermore, the $^{28}\text{Si}(n,\alpha)^{25}\text{Mg}$ reaction channel corresponds to SEEs associated with high deposited energies. For energies below

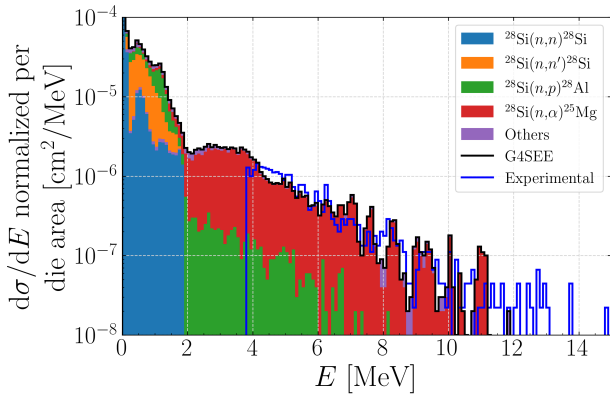


Fig. 5. Comparison between the computational simulations obtained with G4SEE, presenting the four most probable D-T neutron interactions with silicon as a stacked histogram, and the experimental spectrum of the 100 V DMOSFET.

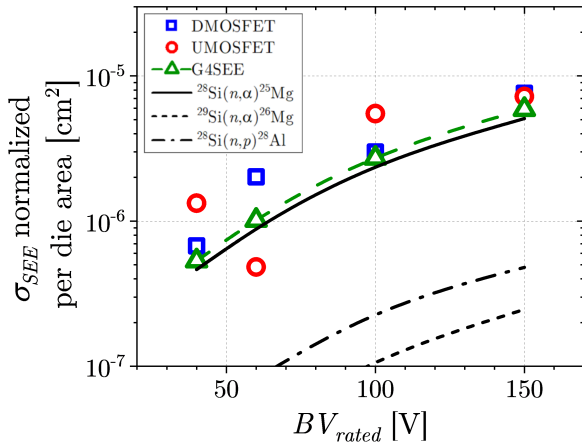


Fig. 6. Experimental and computational neutron-induced SEE cross sections normalized per die area, for energy threshold $E_{th} = 4$ MeV, as a function of the rated drain-source breakdown voltage of the power MOSFETs. The most significant nuclear reaction channels, as determined by computational simulations, are also indicated.

2 MeV, elastic $^{28}\text{Si}(n,n)^{28}\text{Si}$ and inelastic $^{28}\text{Si}(n,n')^{28}\text{Si}$ reaction channels dominate. In the inelastic scattering, the excited compound nucleus emits another neutron with lower energy (n') along with a gamma ray. The deposited energy associated with these reaction channels originates from the recoil of Si, whose energies are constrained by reaction kinematics.

Similar to the approach conducted in Section III-A, the SEE cross sections normalized per die area of the DUTs were quantitatively compared to each other by setting a common energy threshold of $E_{th} = 4$ MeV. Figure 6 shows the experimental normalized SEE cross sections as a function of the nominal drain-source breakdown voltage of the DUTs. The corresponding normalized cross section obtained from computational simulations are included for comparison. Although it cannot be definitively concluded which technology is more susceptible to SEEs induced by D-T neutrons, high-voltage devices generally exhibit greater susceptibility. The computational results follow this trend and show reasonable agreement with experimental data within one order of magnitude. On average, the percentage deviation between computational and experimental results

is approximately 40%, with the largest discrepancy (about a factor of two) occurring for the 60 V UMOSFET. Despite the complexity of the underlying phenomena, this moderate quantitative agreement suggests that the computational model proposed in this paper has potential relevance for neutron-induced SEE rate estimates in power MOSFETs.

The results of this study demonstrate that fast neutrons from a D-T neutron generator can prematurely induce avalanche multiplication effects in UMOSFETs compared to DMOSFETs. Whereas intermediate- to high-voltage UMOSFETs were found susceptible to avalanche induced by D-T neutrons, both low-voltage DMOS and UMOS power FETs were found to be immune to such effects. Since the avalanche multiplication phenomenon is inherently linked to the impact ionization process, it must be highly sensitive to the local electric field intensity [9]. Consequently, the earlier onset of neutron-induced avalanche multiplication in UMOSFETs can be attributed to the significantly stronger electric field intensities near their trench gate corners (as indicated in Fig. 1), compared to those found in similarly rated DMOSFET architectures [30].

During avalanche, the carrier density induced by secondaries, $n(x)$, is multiplied as carriers transverse the electric field \mathcal{E} of the depletion region according to $dn/dx = \alpha(x)n(x)$, where α is the impact ionization rate [32]. Since α strongly depends on the electric field intensity [33], UMOSFETs generally exhibit pronounced avalanche multiplication. To elucidate this phenomenon, at least two distinct conditions can be analyzed: low and high-level carrier injection.

Under low-level injection, the electric field remains unperturbed as carriers drift toward the depletion region. For instance, Fig. 7 qualitatively exemplifies the influence of steady state field on charge collection in UMOSFETs compared to similarly rated DMOSFETs ($BV_{rated} = 30$ V, $BV_{DS} = 42$ V). Under low-field conditions, such as during underbiased operation ($V_{DS} = 10$ V), the electric field intensity in both UMOS and DMOS devices is insufficient to induce significant avalanche multiplication. As a result, approximately the same number of electrons enter and leave the depletion region, *i.e.*, $n(x)/n(0) \approx 1$. In contrast, under high-field conditions, such as in overbias operation ($V_{DS}/BV_{DS} \gtrsim 90\%$), the exponential dependence of impact ionization on field intensity favors avalanche multiplication in UMOSFETs over similarly rated DMOSFETs when operating at $V_{DS}/BV_{DS} = 95\%$. This behavior is also expected to occur in high-voltage devices, where the stronger fields in UMOSFETs further enhance avalanche effects. For instance, the 40 V-100 V devices shown in Fig. 7 operate at a maximum of $V_{DS}/BV_{DS} = 88.7\%$ (60 V DMOSFET), whereas the 150 V devices operate at a minimum of 91.5% (UMOSFET). Since impact ionization rates decrease exponentially with decreasing electric field [34], avalanche multiplication should be weaker for low-voltage devices. Except for strong multiplication observed in 100 V and 150 V UMOS devices, a closer examination of Fig. 4 reveals that measured deposited energies in low-voltage devices slightly exceed computational predictions.

Under high-level injection from secondary ions, the electric field is time-dependent and technology computer-aided design

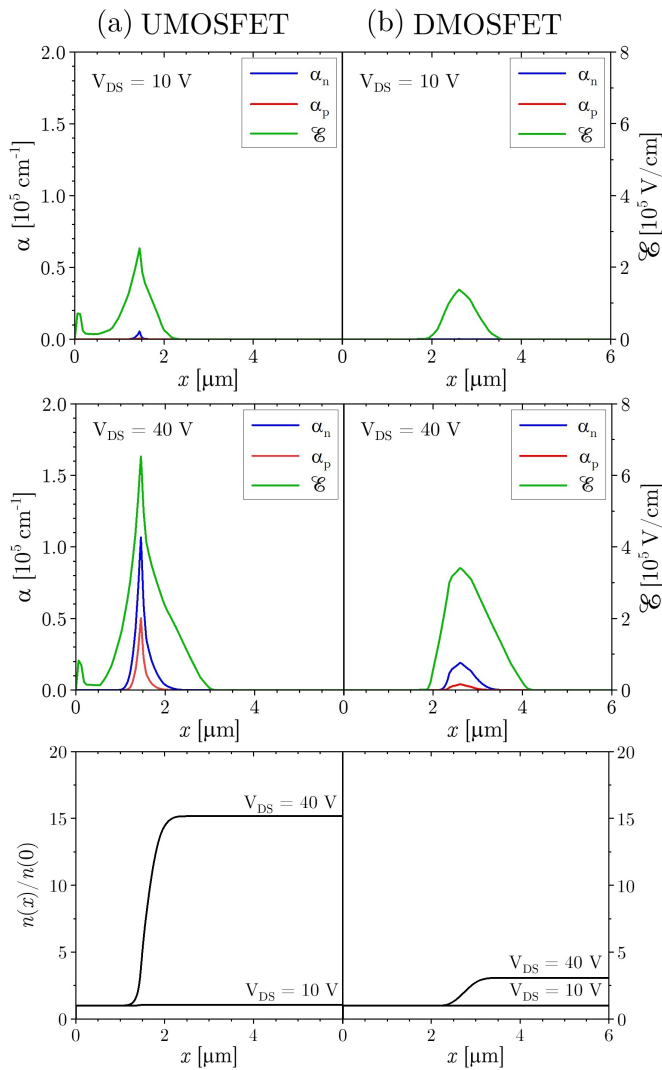


Fig. 7. Electric field intensities (\mathcal{E}), impact ionization rates for the average number of multiplied electrons per primary electron injected into the depletion region in similarly rated (a) UMOFET and (b) DMOFET. The electric field distributions for both 30 V-rated devices, designed with an equivalent breakdown voltage of $BV_{DS} = 42$ V, were extracted from [30]. Impact ionization rates calculated based on [33]. Comparable graphs are presented on the same scale.

(TCAD) simulations can provide valuable insights into its dynamics in UMOSFETs. TCAD simulations of neutron-induced SEEs in a generic 150 V-rated UMOSFET were performed to analyze field dynamics using the ECORCE software [35]. The simulated structure and doping profile were calculated using (3)–(5) and are shown in Fig. 8. The physics models adopted include carrier generation via impact ionization and band-to-band tunneling, recombination (Shockley-Read-Hall and Auger), radiation-induced electron-hole pair separation (yield function), band-gap narrowing, and field- and doping-dependent carrier mobility [35]. For a nuclear reaction $^{28}\text{Si}(n,\alpha)^{25}\text{Mg}$ initiated by a frontal neutron incidence, whether the α particle (ejectile) is emitted at 0° (forward direction), the ^{25}Mg (recoil) must be emitted at 180° (backward direction) to conserve momentum, and vice versa. Particularly for α particle emission at 0°, two-body kinematic calculations

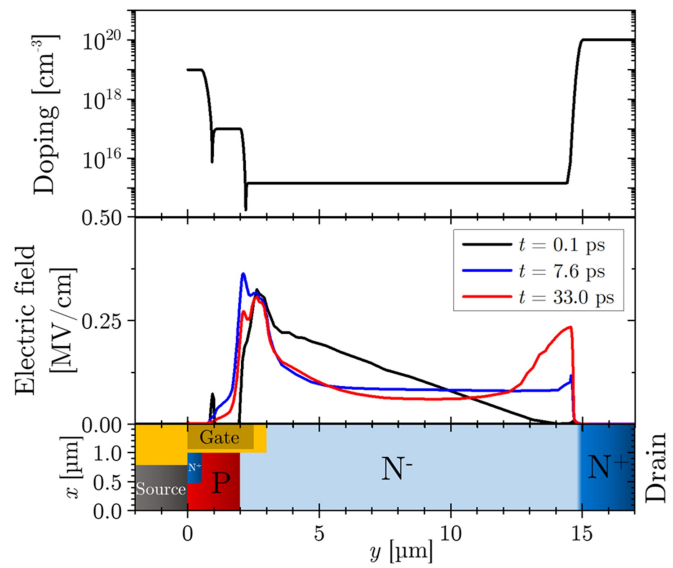


Fig. 8. Doping, electric field, and geometry of a generic 150 V UMOSFET simulated under D-T neutron exposure. Simulated using ECORCE [35].

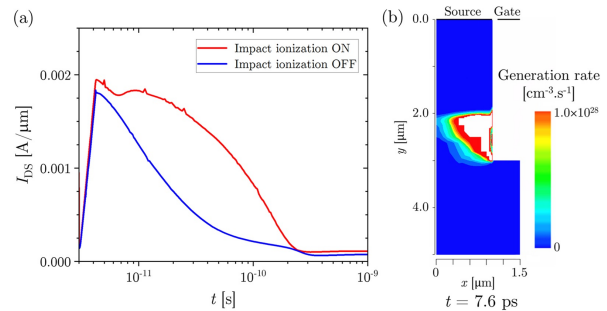


Fig. 9. (a) Influence of impact ionization on the temporal evolution of drain-source current (I_{DS}). (b) Spatial distribution of carrier generation rate concentration near the trench gate corners at peak electric field condition. Simulated using ECORCE [35].

yield recoil and ejectile energies of approximately 0.3 MeV and 11.0 MeV, respectively. Using SRIM code [29], the corresponding particle ranges in Si are estimated at 0.6 μm e 81.5 μm. In our TCAD simulations, the $^{28}\text{Si}(n,\alpha)^{25}\text{Mg}$ reaction was defined to occur near the trench ($x = 0.9$ μm) and below the device surface ($y = 0.6$ μm), in order to ensure integral energy deposition of secondary particles within the device.

Figure 8 shows the temporal evolution of the electric field after a neutron-induced nuclear reaction in the device at $V_{DS} = 150$ V. Under high charge injection from secondary ions, the electric field redistributes in the drift region during avalanche. Through the Egawa effect [36], the field intensities concentrate at the drift region edges, enhancing impact ionization and carrier multiplication due to resulting field. The influence of impact ionization on drain-source current (I_{DS}) is illustrated in Fig. 9, where intense generation rates near the trench corner promote higher collected charge. This mechanism is experimentally confirmed by neutron experiments in Fig. 4, where collected charge exceeds deposited charge without triggering SEBs.

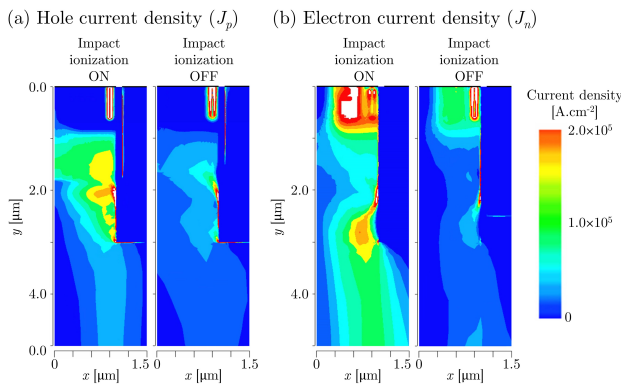


Fig. 10. (a) Hole and (b) electron current density distributions at peak electric field conditions due to neutron-induced nuclear reaction. Simulations compare scenarios with impact ionization model enabled and disabled. When impact ionization is active, significant hole current flows through the p-base region. Simulated using ECORCE [35].

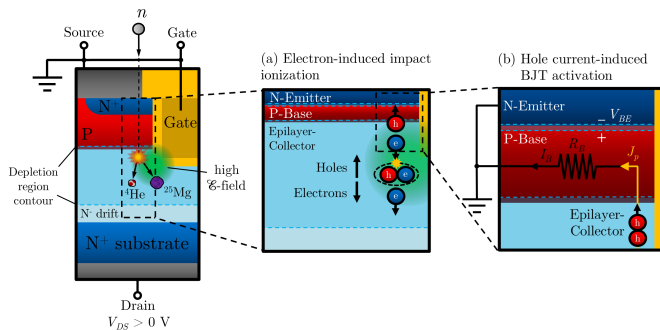


Fig. 11. Mechanism of neutron-induced avalanche multiplication in power UMOSFETs.

Parasitic bipolar junction transistor activation (BJT) can also play an important role in charge multiplication. Figure 10 shows intense hole current densities flowing through the p-base region due to impact ionization, temporarily sustaining electron injection from the n-emitter, and resulting in the second current bump observed in Fig. 9.

Figure 11 summarizes the complete mechanism of neutron-induced avalanche multiplication in UMOSFETs. Secondary charged particles, produced from neutron-induced nuclear reactions, generate dense ionization tracks within the device. When these ionization charge carriers pass near the trench corners, where an intense electric field exists, carrier multiplication via impact ionization process is favored (Fig. 11 (a)). In cases of moderate-gain avalanche, the corresponding hole multiplication current in the p-base region can temporarily activate the parasitic BJT. Similar to DMOSFETs [9], the temporarily activation occur in UMOSFETs when the base current causes a sufficient voltage drop $V_{BE} = R_B I_B$ to forward bias the emitter-base junction (Fig. 11 (b)). Under extreme conditions, the BJT activation can become self-sustaining, ultimately leading to a destructive SEB [32], [37]. Consequently, reducing the electric field stress near trench corners could minimize avalanche multiplication and enhance the reliability of Si UMOSFETs to neutron-induced destructive effects.

The SEB vulnerability of Si UMOSFETs under atmospheric

neutrons has been very recently experimentally verified [21], and this study elucidates the underlying physical mechanisms. As established in the literature, the SEB destructive failure is strongly dependent on the local electric field intensity and ionization impact phenomenon [38]. Our findings confirm that the increased vulnerability of UMOSFETs in terrestrial radiation environments stems from their intrinsic electric field distributions. Additionally, one may argue that secondary ion-induced avalanche multiplication due to intense electric fields in UMOSFETs can potentially favor gate dielectric degradation due to hot carrier injection [6] or SEGR triggering in extreme cases. However, these mechanisms require additional experimental verification.

IV. CONCLUSION

Experimental and computational results confirmed that monoenergetic fast neutrons from D-T neutron generators can induce premature and enhanced avalanche multiplication effects in intermediate- to high-voltage Si UMOSFETs compared to similarly rated DMOSFETs. In contrast, both low-voltage UMOS and DMOS devices exhibit immunity to such effects, producing similar SEE responses. The intense electric field near the UMOS trench corners is found to be the main contributing factor, favoring impact ionization process and leading to observed avalanche multiplication. These findings suggest that neutron-induced avalanche multiplication effects in Si UMOSFETs significantly influence destructive radiation effects that depend on impact ionization, particularly SEBs. Consequently, results help elucidate the fundamental mechanisms behind the vulnerability of Si UMOSFETs to premature destructive failures induced by atmospheric neutrons in terrestrial environment.

REFERENCES

- [1] E. Petersen, *Single Event Effects in Aerospace*. John Wiley & Sons, 2011.
- [2] F.-K. Liu, Z.-L. Liu, and X.-J. Li, "Impact of ^{60}Co - γ irradiation pre-treatment on single-event burnout in n-channel power VDMOS transistors," *IEEE Electron Device Lett.*, vol. 45, no. 7, pp. 1105–1108, Jul. 2024, doi: 10.1109/LED.2024.3403570.
- [3] S. G. Alberton, V. Aguiar, N. H. Medina, N. Added, E. Macchione, R. Menegasso, G. Cesário, H. C. Santos, V. Scarduelli, J. Alcántara-Núñez *et al.*, "Charge deposition analysis of heavy-ion-induced single-event burnout in low-voltage power VDMOS-FET," *Microelectron. Reliab.*, vol. 137, p. 114784, Oct. 2022, doi: 10.1016/j.microrel.2022.114784.
- [4] I. Mouret, P. Calvel, M. Allenspach, J. Titus, C. Wheatley, K. LaBel, M.-C. Calvet, R. Schrimpf, and K. Galloway, "Measurement of a cross-section for single-event gate rupture in power MOSFETs," *IEEE Electron Device Lett.*, vol. 17, no. 4, pp. 163–165, Aug. 1996, doi: 10.1109/55.485161.
- [5] A. Hands, P. Morris, K. Ryden, C. Dyer, P. Truscott, A. Chugg, and S. Parker, "Single event effects in power MOSFETs due to atmospheric and thermal neutrons," *IEEE Trans. Nucl. Sci.*, vol. 58, no. 6, pp. 2687–2694, Dec. 2011, doi: 10.1109/TNS.2011.2168540.
- [6] R. K. Williams, M. N. Darwish, R. A. Blanchard, R. Siemieniec, P. Rutter, and Y. Kawaguchi, "The trench power MOSFET: Part I—History, technology, and prospects," *IEEE Trans. Electron Devices*, vol. 64, no. 3, pp. 674–691, Mar. 2017, doi: 10.1109/TED.2017.2653239.
- [7] D. Ueda, H. Takagi, and G. Kano, "A new vertical power MOSFET structure with extremely reduced on-resistance," *IEEE Trans. Electron Devices*, vol. 32, no. 1, pp. 2–6, Jan. 1985, doi: 10.1109/T-ED.1985.21900.

- [8] R. K. Williams, M. N. Darwish, R. A. Blanchard, R. Siemieniec, P. Rutter, and Y. Kawaguchi, "The trench power MOSFET—Part II: Application specific VDMOS, LDMOS, packaging, and reliability," *IEEE Trans. Electron Devices*, vol. 64, no. 3, pp. 692–712, Mar. 2017, doi: [10.1109/TED.2017.2655149](https://doi.org/10.1109/TED.2017.2655149).
- [9] B. J. Baliga, *Fundamentals of Power Semiconductor Devices*, 2nd ed. Springer International Publishing, 2018.
- [10] J. L. Titus, "An updated perspective of single event gate rupture and single event burnout in power MOSFETs," *IEEE Trans. Nucl. Sci.*, vol. 60, no. 3, pp. 1912–1928, Jun. 2013, doi: [10.1109/TNS.2013.2252194](https://doi.org/10.1109/TNS.2013.2252194).
- [11] K. F. Galloway, "A brief review of heavy-ion radiation degradation and failure of silicon UMOS power transistors," *Electronics*, vol. 3, no. 4, pp. 582–593, Sep. 2014, doi: [10.3390/electronics3040582](https://doi.org/10.3390/electronics3040582).
- [12] Y. Wang, Y. Zhang, and C. Yu, "Research of single-event burnout in power UMOSFETs," *IEEE Trans. Electron Devices*, vol. 60, no. 2, pp. 887–892, Feb. 2013, doi: [10.1109/TED.2012.2234126](https://doi.org/10.1109/TED.2012.2234126).
- [13] Y. Wang, Y. Zhang, L.-G. Wang, and C. Yu, "Single-event burnout hardening of power UMOSFETs with optimized structure," *IEEE Trans. Electron Devices*, vol. 60, no. 6, pp. 2001–2007, Jun. 2013, doi: [10.1109/TED.2013.2256426](https://doi.org/10.1109/TED.2013.2256426).
- [14] Y. Wang, C.-H. Yu, Z. Dou, and W. Xue, "Single-event burnout hardening of power UMOSFETs with integrated schottky diode," *IEEE Trans. Electron Devices*, vol. 61, no. 5, pp. 1464–1469, May 2014, doi: [10.1109/TED.2014.2312948](https://doi.org/10.1109/TED.2014.2312948).
- [15] Y. Wang, C.-H. Yu, M.-S. Li, F. Cao, and Y.-J. Liu, "High-performance split-gate-enhanced UMOSFET with dual channels," *IEEE Trans. Electron Devices*, vol. 64, no. 4, pp. 1455–1460, Apr. 2017, doi: [10.1109/TED.2017.2665589](https://doi.org/10.1109/TED.2017.2665589).
- [16] Y. Wang, C.-H. Yu, X.-J. Li, and J.-Q. Yang, "A comparative study on heavy-ion irradiation impact on p-channel and n-channel power UMOSFETs," *IEEE Trans. Nucl. Sci.*, vol. 69, no. 6, pp. 1249–1256, Jun. 2022, doi: [10.1109/TNS.2022.3175954](https://doi.org/10.1109/TNS.2022.3175954).
- [17] C.-H. Yu, Y. Wang, M.-T. Bao, X.-J. Li, J.-Q. Yang, and F. Cao, "Impact of heavy-ion irradiation in an 80-V radiation-hardened split-gate trench power UMOSFET," *IEEE Trans. Electron Devices*, vol. 69, no. 2, pp. 664–668, Feb. 2022, doi: [10.1109/TED.2021.3135369](https://doi.org/10.1109/TED.2021.3135369).
- [18] Y. Wang, J. Tao, Y. Zhong, X. Zhang, T. Xiong, R. Yin, Y. Zhang, H. Wu, and S. Hu, "Experimental investigation and hardening of single-event gate rupture in 100-V spl-gate trench VDMOS," *IEEE Trans. Nucl. Sci.*, vol. 71, no. 1, pp. 72–79, Jan. 2024, doi: [10.1109/TNS.2023.3345348](https://doi.org/10.1109/TNS.2023.3345348).
- [19] S. G. Alberton, A. C. V. Bôas, N. H. Medina, M. A. Guazzelli, V. A. P. Aguiar, N. Added, C. A. Federico, O. L. Gonzalez, T. C. Cavalcante, E. C. F. Pereira Júnior, and R. G. Vaz, "Alpha particle- and neutron-induced single-event effects in COTS power FETs," in *2022 22nd European Conference on Radiation and Its Effects on Components and Systems (RADECS)*, 2022, pp. 1–4, doi: [10.1109/RADECS55911.2022.10412582](https://doi.org/10.1109/RADECS55911.2022.10412582).
- [20] S. G. Alberton, A. C. V. Bôas, M. A. Guazzelli, J. Wyss, V. A. P. Aguiar, N. Added, C. A. Federico, T. C. Cavalcante, E. C. F. Pereira Júnior, R. G. Vaz, O. L. Gonzalez, L. Silvestrin, S. Mattiazzo, C. Cazzaniga, M. Kastriotou, C. Frost, A. Paccagnella, and N. Medina, "Studies on the Reliability of Power UMOSFETs in the Terrestrial Radiation Environment," submitted and accepted to *2024 24th European Conference on Radiation and Its Effects on Components and Systems (RADECS)*.
- [21] S. G. Alberton, A. C. V. Bôas, J. Wyss, V. A. P. Aguiar, M. S. Pereira, L. Silvestrin, S. Mattiazzo, A. Paccagnella, C. Cazzaniga, M. Kastriotou, C. D. Frost, and N. H. Medina, "On the vulnerability of UMOSFETs in terrestrial radiation environments," *IEEE Access*, vol. 13, pp. 53 885–53 894, Mar. 2025, doi: [10.1109/ACCESS.2025.3553758](https://doi.org/10.1109/ACCESS.2025.3553758).
- [22] D. Lucsányi, R. G. Alía, K. Biľko, M. Cecchetto, S. Fiore, and E. Pirovano, "G4SEE: A Geant4-based single event effect simulation toolkit and its validation through monoenergetic neutron measurements," *IEEE Trans. Nucl. Sci.*, vol. 69, no. 3, pp. 273–281, Mar. 2022, doi: [10.1109/TNS.2022.3149989](https://doi.org/10.1109/TNS.2022.3149989).
- [23] P. McNulty, W. Bearnvais, and D. Roth, "Determination of SEU parameters of NMOS and CMOS SRAMs," *IEEE Transactions on Nuclear Science*, vol. 38, no. 6, pp. 1463–1470, Dec. 1991, doi: [10.1109/23.124133](https://doi.org/10.1109/23.124133).
- [24] S. Kuboyama, S. Matsuda, T. Kanno, and T. Ishii, "Mechanism for single-event burnout of power MOSFETs and its characterization technique," *IEEE Transactions on Nuclear Science*, vol. 39, no. 6, pp. 1698–1703, Dec. 1992, doi: [10.1109/23.211356](https://doi.org/10.1109/23.211356).
- [25] W. Deuchars and G. Lawrence, "Interaction of 14-MeV. neutrons with a silicon semiconductor nuclear particle detector," *Nature*, vol. 191, no. 4792, Sep. 1961, doi: [10.1038/191995a0](https://doi.org/10.1038/191995a0).
- [26] J. K. Tuli and A. Sonzogni, "NNDC data services," Brookhaven National Lab.(BNL), Upton, NY (United States), Tech. Rep., Apr. 2010, doi: [10.2172/1013475](https://doi.org/10.2172/1013475).
- [27] R. Firestone, "Nuclear data sheets for A = 25," *Nuclear Data Sheets*, vol. 110, no. 8, pp. 1691–1744, Aug. 2009, doi: [10.1016/j.nds.2009.06.001](https://doi.org/10.1016/j.nds.2009.06.001).
- [28] M. S. Basunia, "Nuclear data sheets for A = 28," *Nuclear Data Sheets*, vol. 114, no. 10, pp. 1189–1291, Oct. 2013, doi: [10.1016/j.nds.2013.10.001](https://doi.org/10.1016/j.nds.2013.10.001).
- [29] J. F. Ziegler, M. D. Ziegler, and J. P. Biersack, "SRIM—The Stopping and Range of Ions in Matter (2010)," *Nuclear Instruments and Methods in Physics Research Section B: Beam Interactions with Materials and Atoms*, vol. 268, no. 11–12, pp. 1818–1823, 2010, doi: [10.1016/j.nimb.2010.02.091](https://doi.org/10.1016/j.nimb.2010.02.091).
- [30] B. J. Baliga, *Advanced Power MOSFET Concepts*. Springer Science & Business Media, 2010.
- [31] S. Agostinelli, J. Allison, K. Amako, J. Apostolakis, H. Araujo, P. Arce, M. Asai, D. Axen, S. Banerjee, G. Barrand *et al.*, "Geant4—a simulation toolkit," *Nucl. Instrum. Methods Phys. Res. A*, vol. 506, no. 3, pp. 250–303, Jul. 2003, doi: [10.1016/S0168-9002\(03\)01368-8](https://doi.org/10.1016/S0168-9002(03)01368-8).
- [32] J. H. Hohl and K. F. Galloway, "Analytical model for single event burnout of power MOSFETs," *IEEE Trans. Nucl. Sci.*, vol. 34, no. 6, pp. 1275–1280, Dec. 1987, doi: [10.1109/TNS.1987.4337465](https://doi.org/10.1109/TNS.1987.4337465).
- [33] R. Van Overstraeten and H. De Man, "Measurement of the ionization rates in diffused silicon p-n junctions," *Solid-State Electronics*, vol. 13, no. 5, pp. 583–608, May 1970, doi: [10.1016/0038-1101\(70\)90139-5](https://doi.org/10.1016/0038-1101(70)90139-5).
- [34] A. G. Chynoweth, "Ionization rates for electrons and holes in silicon," *Physical Review*, vol. 109, no. 5, p. 1537, 1958.
- [35] A. Michez, S. Dhombres, and J. Boch, "ECORCE: A TCAD tool for total ionizing dose and single event effect modeling," *IEEE Trans. Nucl. Sci.*, vol. 62, no. 4, pp. 1516–1527, Aug. 2015, doi: [10.1109/TNS.2015.2449281](https://doi.org/10.1109/TNS.2015.2449281).
- [36] H. Egawa, "Avalanche characteristics and failure mechanism of high voltage diodes," *IEEE Trans. Electron Devices*, vol. ED-13, no. 11, pp. 754–758, Nov. 1966, doi: [10.1109/T-ED.1966.15838](https://doi.org/10.1109/T-ED.1966.15838).
- [37] J. Hohl and G. Johnson, "Features of the triggering mechanism for single event burnout of power MOSFETs," *IEEE Trans. Nucl. Sci.*, vol. 36, no. 6, pp. 2260–2266, Dec. 1989, doi: [10.1109/23.45433](https://doi.org/10.1109/23.45433).
- [38] S. Kuboyama, N. Ikeda, T. Hirao, and S. Matsuda, "Improved model for single-event burnout mechanism," *IEEE Trans. Nucl. Sci.*, vol. 51, no. 6, pp. 3336–3341, Dec. 2004, doi: [10.1109/TNS.2004.839512](https://doi.org/10.1109/TNS.2004.839512).